Evaluation of Oxygen Plasma and UV Ozone Methods for Cleaning of Occluded Areas in MEMS Devices

D. Adam Hook, James A. Ohlhausen, Jacqueline Krim, and Michael T. Dugger

***Abstract*—UV ozone and oxygen plasma treatments are two common procedures for cleaning silicon surfaces. The extent to which hidden surfaces of microelectromechanical systems (MEMS) are cleaned by these methods has not been well documented. To probe and compare the effectiveness of the two methods for cleaning occluded regions in MEMS, devices consisting of large movable flaps were fabricated to produce hidden surfaces whose occluded regions exceeded the aspect ratios that typically occur in MEMS devices. The gaps between the flap and the substrate in the custom flap devices were designed to be variable in extent. Their interior regions were initially coated with chemisorbed monolayers and then subjected to cleaning. Both techniques removed monolayers on exposed surfaces and both, to some extent, removed monolayers present on the occluded surfaces. Oxygen plasma was found to be a far more effective method for cleaning the occluded surfaces than the UV ozone method. However, in occlusions with exceptionally large aspect ratios of 1700 : 1, even oxygen plasma could not remove all traces of the chemisorbed monolayers. [2009-0103]**

***Index Terms*—Cleaning procedures, FOTAS, organic monolayer coating, oxygen plasma, surface preparation, TOF-SIMS, UV ozone.**

I. Introduction

THE dominant effects of surface forces on the operation of microelectromechanical systems (MEMS) necessitate control of the surface chemistry to control and mitigate these forces [1]. Cleaning is an important part of surface chemistry control, as attachment of chemisorbed monolayer films relies upon exposure of the desired coating molecules to a surface with known termination [1]. Variations in MEMS fabrication processes, for example, can result in a wide range of post-production surface chemistries while surface contamination routinely occurs during device storage and/or operation. Physisorbed layers of hydrocarbons and water moreover condense onto surfaces in both vacuum and ambient conditions [2]–[4], and they are frequently not removed by simple exposure to ultra-high vacuum conditions [5]. UV ozone and oxygen plasma are two common methods used to clean and/or oxidize MEMS surfaces, particularly those with aluminum (mirror), gold (electrical switch), and silicon (mechanical interface) surfaces [5]–[15]. UV ozone cleaning procedures for semiconductor materials were in use as early as 1972 [7]. In this technique, atmospheric air is exposed to UV light. Oxygen in the air absorbs UV light at 185 nm creating highly active ozone. This ozone adsorbs UV light at 253.7 nm to form atomic oxygen. These react with surface organics to produce carbon-oxygen-based products which desorb from the surface. Oxygen plasma techniques have been used for removal of organics in vacuum deposition techniques since the late 1950s [6]. Here, plasmas generated in subatmospheric pressures of oxygen create highly reactive ions which bombard a surface and react with organics forming volatile species (e.g., CO). These plasmas also contain significant kinetic energies, therefore colliding with a surface can also sputter-etch them [15]. While a variety of studies have been performed that focus on the effectiveness of these techniques for cleaning exposed surfaces of common MEMS materials, the extent to which occluded surfaces are cleaned has to date not been well documented.

The relative effectiveness of oxygen plasma and UV ozone for cleaning occluded and open areas of silicon MEMS devices are investigated here. MEMS devices with large movable flaps were fabricated to include occluded regions that far exceed typical aspect ratios. The flaps were held closed during cleaning, and could be opened afterward to reveal areas that were occluded during the cleaning processes. The devices were coated with a chemically bonded monolayer of tridecafluorotris(dimethylamino)silane, $CF_3(CF_2)_5(CH_2)_2Si(N(CH_3)_2)_3$ or FOTAS before the cleaning treatment. Surface analysis using time-of-flight secondary ion mass spectrometry (ToF-SIMS) was performed on the surfaces after the flaps were opened to assess the effectiveness of the cleaning method. Both techniques effectively removed the FOTAS layer on exposed surfaces. Oxygen plasma was found to be a far more effective method for cleaning the occluded regions than the UV ozone method. It removed all traces of the chemisorbed layer except in occluded areas having exceptionally large aspect ratios of 1700 : 1.

Manuscript received April 24, 2009; revised December 10, 2009; accepted December 14, 2009. Date of publication September 20, 2010; date of current version November 30, 2010. Funding for this project came in part from the AFOSR Extreme Friction MURI F49620-01-1-0381 and in part from Sandia National Laboratories, operated by Sandia Corporation, for the U.S. Department of Energy's National Nuclear Security Administration under contract DE-AC04-94AL85000. Subject Editor G. Stemme.

D. A. Hook and J. Krim are with the Department of Physics, North Carolina State University, Raleigh, NC 27695 USA (e-mail: d.adam.hook@gmail.com; jkrim@ncsu.edu).

J. A. Ohlhausen and M. T. Dugger are with the Materials Science and Engineering Center, Sandia National Laboratories, Albuquerque, NM 87185 USA (e-mail: jaohlha@sandia.gov; mtdugge@sandia.gov).

Color versions of one or more of the figures in this paper are available online at http://ieeexplore.ieee.org.

Digital Object Identifier 10.1109/JMEMS.2010.2067193

1057-7157/$26.00 © 2010 IEEE

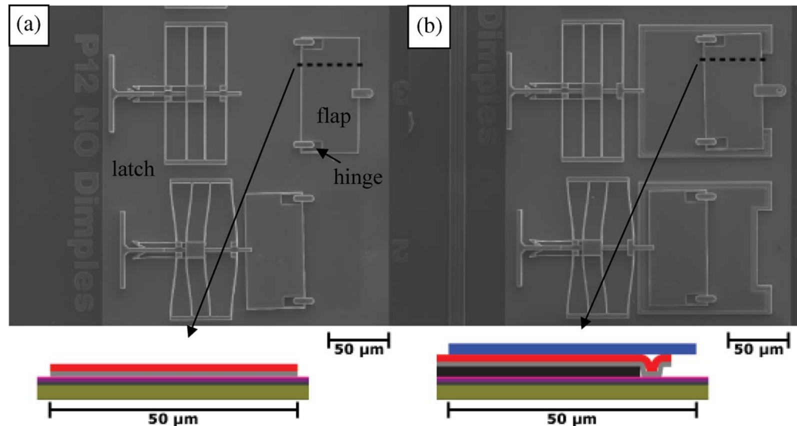

Fig. 1. Scanning electron micrographs of (a) device 1 and (b) device 3 in the as-fabricated (upper) and flipped (lower) states with cross sections in the as-fabricated position. The cross-sections show polySi layers as gray, red, and blue, while the sacrificial oxide is black, and the other layers represent the wafer substrate and dielectric stack.

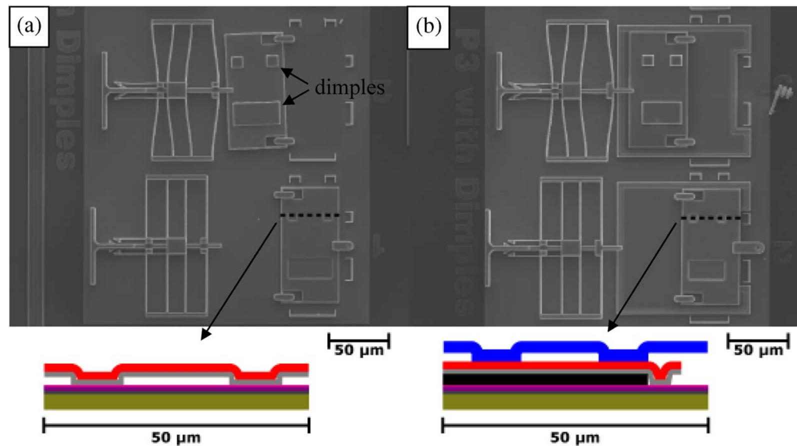

Fig. 2. Scanning electron micrographs of (a) device 2 and (b) device 4 in the as-fabricated (lower) and flipped (upper) states with cross sections in the as-fabricaterd position. The cross-sections show polySi layers as gray, red, and blue, while the sacrificial oxide is black, and the other layers represent the wafer substrate and dielectric stack.

II. Experiment Setup

A. MEMS Flap Structure Fabrication and Monolayer Treatment

Figs. 1 and 2 show SEM images along with cross sections of the four styles of MEMS flap devices employed for these studies. All four devices have flaps with dimensions of 50×100 μm that can be flipped over to reveal areas that are occluded after release. The structures include hinges to assist in the flipping process as well as latches to hold the flaps in place for surface analysis. The structures were designed and fabricated at Sandia National Laboratories, and have been used in the past to assess the ability of vapor deposited monolayers to penetrate into occluded areas of MEMS structures [16]. The devices are fabricated using Sandia National Laboratories' SUMMiT V surface micromachining technology [17] and are constructed from layers of polycrystalline silicon separated by sacrificial layers of silicon dioxide that are subsequently removed. Each layer can be patterned and etched, allowing complex structures to be fabricated.

Fig. 1(a) and (b) shows SEM images and cross sections of devices 1 and 3, respectively. Each SEM image in Fig. 1 contains two identical flap structures. The upper device is shown in its as-fabricated state and the bottom device shows the overturned flaps latched and ready for analysis. The flap on device 1 was fabricated from the poly 12 (P12) layer and the flap on device 2 was fabricated from the poly 3 (P3) layer. After release both rest flat on their respective underlayers, i.e., poly 0 (P0) for device 1 and poly 2 (P2) for device 3, as can be seen from the cross section schematics below the SEM images in Fig. 1. Fig. 2(a) and (b) shows SEM images and cross sections of devices 2 and 4, respectively. Each SEM image shows two identical devices, in this case with the bottom device in the as-fabricated state and the top device showing the flap turned over and latched into place. Devices 2 and 4 are identical to devices 1 and 3, respectively, except for the presence of dimples on their undersides which prop them up so that the bottom of the flap in device 2 sits approximately 1.49 μm above the P0 layer and the flap in device 4 sits approximately 1.63 μm above the P2 layer this is the gap height for both devices.

The minimum distance from the center of the flaps in devices 2 and 4 to the edge (25 μm), divided by the distance between the bottom of the flaps and the substrates, yield minimum gap aspect ratios of 17 : 1 and 15 : 1, respectively. These

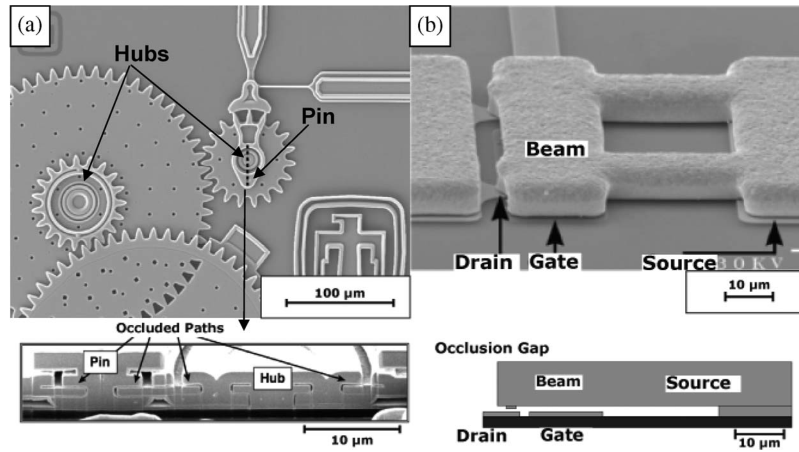

Fig. 3. Scanning electron micrograph of (a) Sandia's microengine and gear train [18], [20], and (b) Northeastern University's cantilever RF-MEMS switch [19].

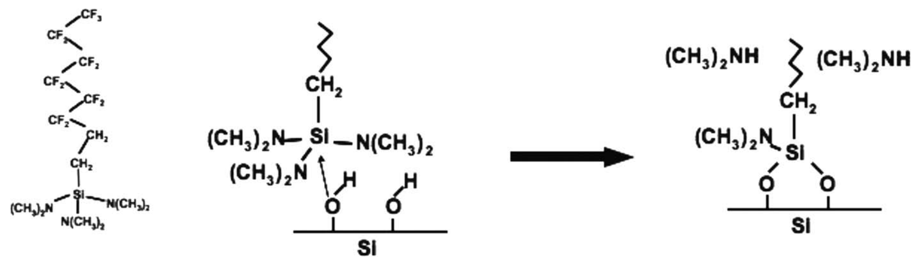

Fig. 4. Schematic representation of the FOTAS reaction with a hydroxilated silicon surface.

aspect ratios are less than that typically seen in MEMS gear-hub structures shown in Fig. 3(a), where gap aspect ratios are on the order of 100 : 1. Devices 2 and 4 therefore represent relatively open structures. However, the flaps do have gap aspect ratios typical of RF switches such as the device shown in Fig. 3(b) having aspect ratio of 10 : 1. In devices 1 and 3, some of the SUMMiT V design rules were intentionally violated to create gaps with extremely high aspect ratio. After release, the bottom of the flaps rest directly on the layer of polycrystalline silicon below and the gap is defined by the roughness of both surfaces. Atomic force microscopy measurements of the P0 surface and the bottom of P12 give an RMS roughness of 1.6 ± 0.1 nm and an asperity radius of approximately 480 ± 100 nm. Using only the gravitational force to prescribe the load ($\sim$1 nN) between the flap and the underlying substrate, a Greenwood-Williamson contact mechanics model gives a mean plane separation (gap) of approximately 14 nm. Therefore in devices 1 and 3, the minimum gap aspect ratio is 1700 : 1 [21]. Inclusion of the adhesion forces that are undoubtedly present would decrease the gap and create an even larger aspect ratio. As an example, if an adhesion force of 1 μN is included, the gap drops to 11 nm and the aspect ratio increases to 2230 : 1.

The fabrication and etch process for SUMMiT V devices has been described in detail previously [17]. Briefly, the sacrificial oxide was removed using an aqueous HF etch. They were then rinsed in deionized water and transferred to methanol which was supercritically extracted in CO_2 to avoid irreversible adhesion of the structures arising from liquid capillary forces. The devices were then transferred to a vacuum chamber for surface preparation and monolayer deposition. The devices were cleaned using an O_2/H_2O plasma and coated with a monolayer of tridecafluorotris(dimethylamino)silane, $CF_3(CF_2)_5(CH_2)_2Si(N(CH_3)_2)_3$ or FOTAS. The dimethylamino groups can react exothermically with surface hydroxyl groups and afford the potential for up to three covalent bonds with the surface per molecule, as illustrated schematically in Fig. 4. This process results in a water contact angle by sessile drop of approximately 110°. A complete description of the monolayer treatment process can be found elsewhere [20]. ToF-SIMS indicates that this coating process results in a surface coverage of approximately 2.5×10^{14} molecules/cm^2 on all surfaces exposed to the vapor, including areas of occlusion [16]. This chemisorbed monolayer was then used as the controlled "contamination" layer that was subsequently used to evaluate the cleaning efficiency of UV ozone and oxygen plasma treatments. This particular layer was chosen because of its uniform coverage in open as well as in occluded areas. In addition, it is more thermally stable in oxidizing environments than other similar hydrocarbon-based SAM layers [22]. Finally, its chemical bond to the surface makes it more difficult to remove than any heterogenous hydrocarbons deposited from the atmosphere. Therefore, if either of the cleaning procedures employed here remove the layer, then they are assured to remove hydrocarbons.

B. Cleaning Processes and ToF-SIMS Analysis

In the UV Ozone cleaning process, a MEMS die containing all four test devices coated in FOTAS was placed in an aluminum foil-lined Petri dish and placed in a UV ozone

cleaner (Jelight model 144AX) for 15 min along with the lid for the dish. After cleaning, the dish was covered and carried to a probe station. There, the flaps were manually turned over using tungsten whisker probes (Signatone model SE-20T) and latched into place. After all flaps were turned over to expose the occluded areas, the die was placed back in the Petri dish, covered and transferred to the ToF-SIMS chamber for analysis. MEMS devices were placed in dishes containing Al foil in hopes that during transfer between the cleaning equipment and the surface analysis chamber, the cleaned foil would act as a strong adsorber of contaminants that would otherwise desorb and potentially deposit on the MEMS surfaces.

The oxygen plasma cleaning process was similar to that for UV Ozone. A die containing all four test devices coated in FOTAS was placed in a foil-lined Petri dish and placed in an RF oxygen plasma cleaner (Yield Engineering, model Glen-R3A). The chamber was then evacuated and the oxygen plasma cleaning process commenced at 400 W in 110–115 mTorr of oxygen for 5 min. Once cleaned, the devices were again transferred to the probe station, the flaps turned over and latched into place and then taken to the ToF-SIMS analysis chamber. Both of these techniques reflect standard conditions used in cleaning of structures and representative surfaces.

Another MEMS die was placed in a foil-lined Petri dish, but did not go through any cleaning processes. The devices on this die were analyzed for comparison.

The ToF-SIMS monolayer analysis technique used in this study has been described thoroughly elsewhere [16]. Briefly, a Physical Electronics TRIFT I ToF-SIMS system was used to generate positive secondary ion spectral images using a 25 kV ^{69}Ga^{+} primary ion beam rastered over an area of $140 \times 140\ \mu\mathrm{m}^2$. To completely cover the full area of the flaps, four separate scans were acquired and the images concatenated together to form a spectral image montage. The montaged spectral image was then processed using Automated eXpert Spectral Imaging Analysis (AXSIA), a multivariate analysis routine developed at Sandia National Laboratories. It works by fitting self-generated spectral shapes to the data using least squares procedures and the number of chemical components is estimated through an eigenanalysis of the data cross-product matrix, essentially finding the minimum number of chemical components required to fully describe the spectral image [23]. Fig. 5 shows an optical image of the four devices flipped, latched into place, and ready for SIMS analysis. The boxes indicate the entire analysis area.

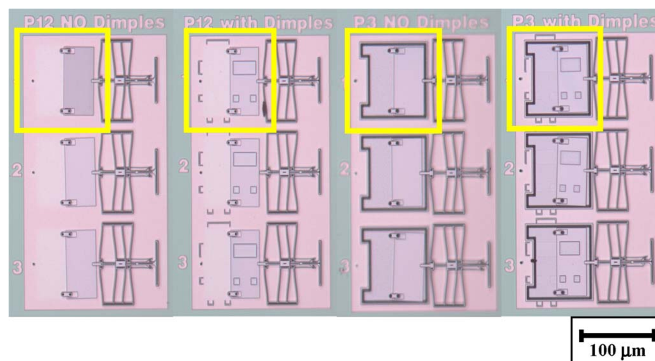

Fig. 5. Optical microscope image of (from left to right) flap devices 1, 2, 3, and 4. Flaps are shown flipped and latched into place. Yellow boxes indicate ToF-SIMS analysis areas for each device.

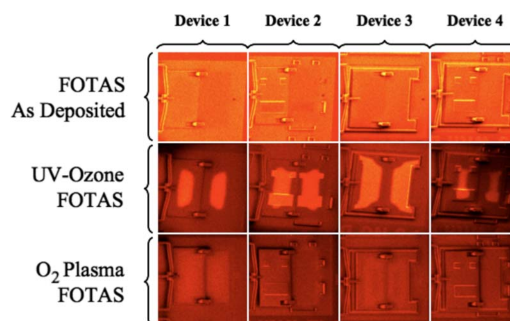

Fig. 6. ToF-SIMS mean ion image montage of flaps as-deposited with FOTAS, UV Ozone cleaned, and O_2 plasma cleaned. Each flap has been turned over and latched into place. Each analysis area is $140 \times 140\ \mu\mathrm{m}^2$. Contrast in this image originates both from chemical differences and from topography, allowing easy identification of the structures in the analysis.

III. Experimental Results and Discussion

Fig. 6 shows the ToF-SIMS mean ion image montage for each of the four tested devices on each of the three die. The flaps are shown flipped over and latched into place. The latch structures can be seen on the left side of the flaps. AXSIA resolved two components of interest and these are presented in Figs. 7 and 8. Fig. 7 shows the spatial locations of a "FOTAS" component in each of the analysis areas shown in Fig. 5, along with the corresponding ion spectrum. Bright pixels correspond to areas with high concentration of this component, while in the dark areas, this component is absent. The FOTAS signature is dominated by C_xF_y fragments originating from the fluorocarbon backbone of the monolayer. It is clear that both the UV Ozone and O_2 plasma cleaning techniques remove all of the FOTAS from the exposed surfaces of the entire flap structure. The figure shows that UV Ozone leaves significant amounts of FOTAS in the occluded areas, corresponding to where the flaps covered the substrate when the devices were treated with FOTAS. Matching patterns of FOTAS can be observed on the bottom of the opened flaps, and on the corresponding areas of the substrate that were covered during FOTAS treatment. The most residual FOTAS is present on device 3 while in contrast most of the FOTAS were removed under device 4. Here, the UV Ozone appears to have removed the FOTAS approximately 18 μm into the occlusion. In device 2, which has the same general geometry but is fabricated by layers closer to the P0 layer and has a slightly higher aspect ratio, the penetration depth was only about 10 μm. UV Ozone's inability to penetrate can be attributed to its fairly short mean free path at atmospheric pressure (11 nm at 760 Torr (1 atm) using the kinetic theory of gases). The classical phenomenological model of diffusion shows a direct relation between the mean free path and the diffusion coefficient [24]. A short mean free path (i.e., small diffusion coefficient) makes it difficult for the ozone and reactive oxygen generated outside of the gap to diffuse deeply into the gap before colliding with other gas molecules, losing energy and recombining to form less reactive molecular

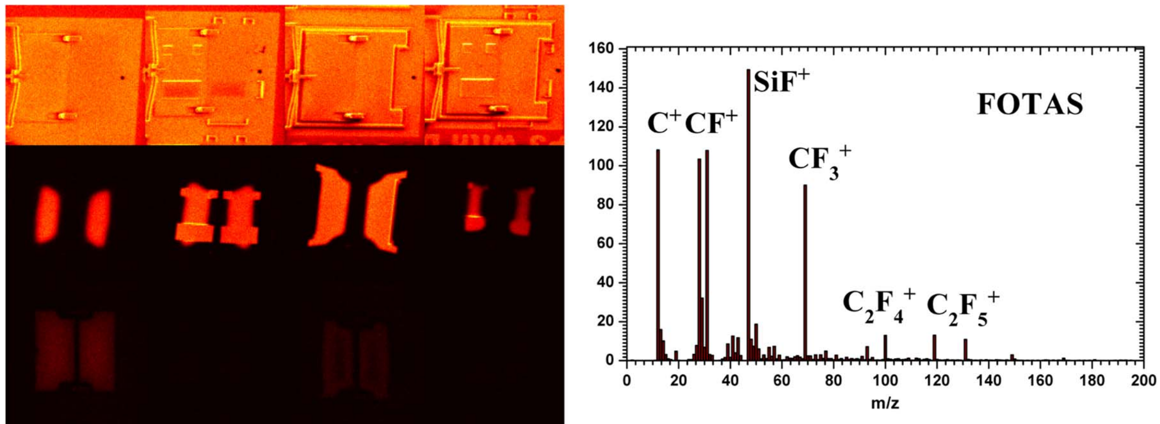

Fig. 7. AXSIA analysis of the die montage showing the FOTAS component. Device numbers and cleaning processes correspond to the relative placements in Fig. 6.

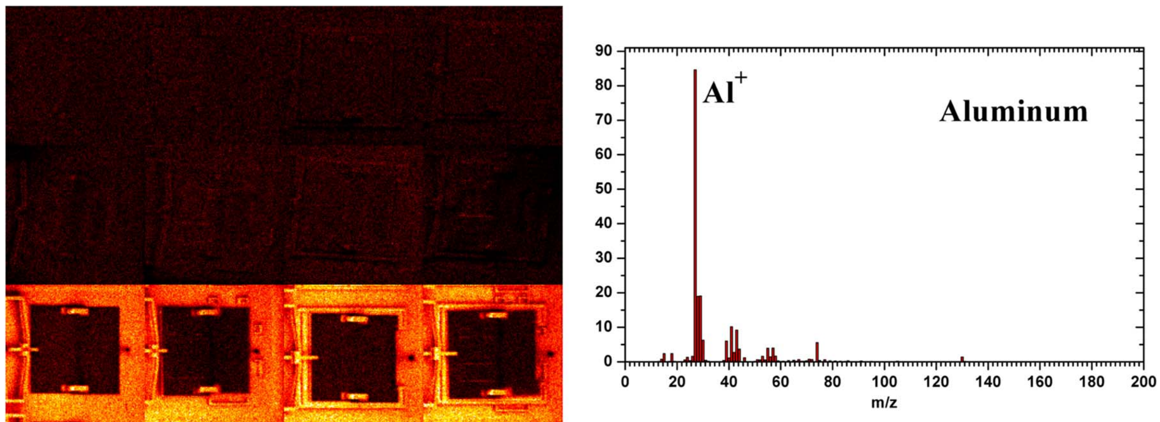

Fig. 8. AXSIA analysis of the die montage showing an aluminum component. Device numbers and cleaning processes correspond to the relative placements in Fig. 6. Only the O_2 plasma cleaning technique showed any trace of aluminum. Aluminum is only seen in exposed areas of the device.

oxygen, i.e., limiting the lifetime of the generated ozone and oxygen radicals when they travel into the occlusion. Lowering the total pressure in the UV Ozone environment would increase the mean free path and likely allow deeper penetration into the occlusion. Another factor that affects the ability of UV Ozone processes to clean is the percentage of molecular oxygen present in the air. An increased molecular oxygen concentration would lead to higher ozone and atomic oxygen concentrations that would likely increase the cleaning efficiency and possibly, the penetration depth. However, in our particular UV Ozone cleaner, controlled variations in total pressure and oxygen concentration are not available. Variations in surface roughness and the state of the flap before cleaning make it difficult to draw quantitative conclusions about penetration depth of UV Ozone from the ToF-SIMS data, but it is clear that UV Ozone cleaning in air is not capable of removing carbonaceous contaminants from high aspect ratio occlusions.

The O_2 plasma cleaning technique showed vastly superior cleaning capabilities to that of UV Ozone. After cleaning for only 5 min, no FOTAS was seen inside of the relatively open occlusions of devices 2 and 4, and only trace amounts were observed in the high aspect ratio occlusions of devices 1 and 3. Here, it is probable that increasing the cleaning time for the O_2 plasma by as little as 5 min could completely clean the devices with high aspect ratio gaps. The mean free path of oxygen ions at 100 mTorr, neglecting additional energy generated by the ionization process, is 140 μm. This is significantly higher than that of UV Ozone at atmospheric pressure and allows diffusion throughout the deep occlusions. While simulation of reactive ion trajectories down deep trenches would need to be conducted for a thorough discussion of the limits of this technique, it is clear that these aspect ratios have not yet reached this limit. The increased kinetic energy of oxygen ions in plasmas can also sputter-clean surfaces, whereas UV Ozone only has a reactive cleaning component. However, this sputtering process can potentially have negative consequences. The ToF-SIMS data shows an aluminum component in the spectral images for O_2 plasma-cleaned devices, as shown in Fig. 8. No aluminum is seen in the as-deposited FOTAS die or the UV Ozone cleaned die, ruling out aluminum deposition from outside influences or deposition in the ToF-SIMS chamber. The O_2 plasma cleaned die exhibit aluminum deposition on all exposed surfaces, but not in the occlusions, consistent with line-of-sight physical vapor deposition. The aluminum may have originated from the foil lining the Petri dish in which the die was sitting or from the oxygen plasma cleaning chamber electrodes since it is known that plasma can sputter metals from the generating electrodes [6], [15]. Therefore, when using O_2 plasma to clean MEMS, care should be taken to ensure that the plasma power used does not generate metals from the plasma electrodes or surrounding

materials or that the sputtered species are not detrimental to the MEMS device operation by changing surface chemistry or shorting electrical connections. An optimum plasma power should be found that removes the undesired contamination species but does not result in the deposition of foreign sputtered materials.

IV. Summary

Oxygen plasma and UV Ozone cleaning techniques were used to remove FOTAS molecules from flap test structures designed to mimic exposed and high-aspect ratio occluded areas. Both UV Ozone and O_2 plasma remove FOTAS from exposed surfaces of silicon MEMS. UV Ozone cleaning (15 mi in 1 atm of air) fails to penetrate into deep occlusions. The O_2 plasma conditions used (400 W in 110–115 mTorr of oxygen for 5 min) resulted in penetration into occlusions better than UV Ozone, completely removing all traces of FOTAS from underneath relatively open geometries while leaving trace amounts of FOTAS underneath extremely high aspect ratio occlusions. However, these conditions also left behind residual aluminum deposits.

References

[1] R. Maboudian and C. Carraro, “Surface engineering for reliable operation of MEMS devices,” *J. Adhesion Sci. Technol.*, vol. 17, no. 4, pp. 583–592, Apr. 2003.

[2] V. Panella, R. Chiarello, and J. Krim, “Adequacy of the Lifshitz theory for certain thin adsorbed films,” *Phys. Rev. Lett.*, vol. 76, pp. 3606–3609, May 1996.

[3] J. Krim, J. G. Dash, and J. Suzanne, “Triple point wetting of light molecular gases on Au(111) surfaces,” *Phys. Rev. Lett.*, vol. 52, pp. 640–643, Feb. 1984.

[4] J. Krim, E. T. Watts, and J. Digel, “Slippage of simple liquid films adsorbed on silver and gold substrates,” *J. Vac. Sci. Tech. A*, vol. 8, pp. 3417–3520, Jan. 1990.

[5] M. Walker, C. Nordquist, D. Czaplewski, G. Patrizi, N. McGruer, and J. Krim, “Impact of in situ oxygen plasma cleaning on the resistance of Ru and Au-Ru based RF microelectromechanical system contacts in vacuum,” *J. Appl. Phys.*, vol. 107, p. 084509, Apr. 2010.

[6] L. Holland, *Vacuum Deposition of Thin Films*. New York: Wiley, 1960.

[7] D. A. Bolon and C. O. Kunz, “Ultraviolet depolymerization of photoresist polymers,” *Polym. Eng. Sci.*, vol. 12, no. 2, pp. 109–111, Mar. 1972.

[8] A. B. Frazier, H. A. Chong, and M. G. Allen, “Development of micromachined devices using polyimide-based processes,” *Sens. Actuators A, Chem.*, vol. 45, no. 1, pp. 47–55, Oct. 1994.

[9] K. Arita, K. Noda, and T. Asano, “Charge build-up and its reduction in plasma cleaning process,” in *Proc. IEEE/CPMT Berlin Int. Electron. Manuf. Technol. Symp.*, Apr. 1998, pp. 92–97.

[10] A. Tran, Y. H. Lo, Z. H. Zhu, D. Haronian, and E. Mozdy, “Surface micromachined Fabry-Perot tunable filter,” *IEEE Photon. Technol. Lett.*, vol. 8, no. 3, pp. 393–395, Mar. 1996.

[11] M. Bartek and R. F. Wolffenbuttel, “Dry release of metal structures in oxygen plasma: Process characterization and optimization,” *J. Micromech. Microeng.*, vol. 8, no. 2, pp. 91–94, Jun. 1998.

[12] S. E. Lin, “A surface analysis on oxygen plasma-cleaned gold pattern-plated substrates for wire bondability,” *Surf. Coat. Technol.*, vol. 173, no. 1, pp. 47–57, Aug. 2003.

[13] A. Yu, A. Q. Liu, J. Oberhammer, Q. X. Zhang, and H. M. Hosseini, “Characterization and optimization of dry releasing for the fabrication of RF MEMS capacitive switches,” *J. Micromech. Microeng.*, vol. 17, no. 10, pp. 2024–2030, Sep. 2007.

[14] W. Kern and K. A. Reinhardt, *Handbook of Silicon Cleaning Technology*. Norwich, NY: William Andrew, 2008.

[15] J. L. Vossen, “The preparation of substrates for film deposition using glow discharge techniques,” *J. Phys. E, Sci. Instrum.*, vol. 12, no. 3, pp. 159–167, Mar. 1979.

[16] J. A. Ohlhausen and K. R. Zavadil, “Time-of-flight secondary ion mass spectrometry measurements of a fluorocarbon-based self-assembled monolayer on Si,” *J. Vac. Sci. Technol. A, Vac. Surf. Films*, vol. 24, no. 4, pp. 1172–1178, Jul. 2006.

[17] J. J. Sniegowski and M. P. de Boer, “IC-compatible polysilicon surface micromachining,” *Annu. Rev. Mater. Sci.*, vol. 30, pp. 299–333, Aug. 2000.

[18] [Online]. Available: http://mems.sandia.gov/gallery/images

[19] S. Majumder, N. E. McGruer, G. G. Adams, P. M. Zavracky, R. H. Morrison, and J. Krim, “Study of contacts in an electrostatically actuated microswitch,” *Sens. Actuators A, Phys.*, vol. 93, no. 1, pp. 19–26, Aug. 2001.

[20] M. G. Hankins, P. J. Resnick, P. J. Clews, T. M. Mayer, D. R. Wheeler, D. M. Tanner, and R. A. Plass, “Vapor deposition of amino-functionalized self-assembled monolayers on MEMS,” *Proc. SPIE*, vol. 4980, pp. 238–247, 2003.

[21] J. A. Greenwood and J. B. P. Williamson, “Contact of nominally flat surfaces,” *Philos. Trans. Roy. Soc. London A, Math. Phys. Sci.*, vol. 295, no. 1442, pp. 300–319, Dec. 1966.

[22] M. T. Dugger, R. J. Hohlfelder, and D. E. Peebles, “Degradation of monolayer lubricants for MEMS,” in *Proc. SPIE—Int. Soc. Opt. Eng.*, 2003, vol. 4980, pp. 138–150.

[23] J. A. Ohlhausen, M. R. Keenan, P. G. Kotula, and D. E. Peebles, “Multivariate statistical analysis of time-of-flight secondary ion mass spectrometry images using AXSIA,” *Appl. Surf. Sci.*, vol. 231/232, pp. 230–234, Jun. 2004.

[24] E. L. Cussler, *Diffusion: Mass Transfer in Fluid Systems*. Cambridge, U.K.: Cambridge Univ. Press, 1997.

D. Adam Hook received the B.S. degree in physics from North Carolina State University, Raleigh, in 2003, where he is currently working toward the Ph.D. degree in physics.

For three summers, he was a Student Intern with the Microsystem Materials Division, Sandia National Laboratories, Albuquerque, NM. He has been the President of the Graduate Physics Students Association as well as the University Graduate Student Association Representative for the Department of Physics, North Carolina State University. His research interests include vapor phase lubrication of MEMS, MEMS design, microtribology, surface analysis, and scanning electron microscopy.

James A. Ohlhausen received the B.S. degree in chemistry from Abilene Christian University, Abilene, TX, in 1990, and the M.S. degree in materials engineering from the New Mexico Institute of Mining and Technology, Socorro, in 2004.

He is currently a Member of Technical Staff with the Materials Characterization Department, Sandia National Laboratories, Albuquerque, NM. He is with the Surface Analysis Laboratory, performing surface analysis for his customers using ToF-SIMS, AES, XPS, AFM, and synchrotron techniques. His current research interests include data extraction and advanced acquisition methods.

Jacqueline Krim received the B.A. degree in physics from the University of Montana, Missoula, in 1978, and the Ph.D. degree in experimental condensed matter physics from the University of Washington, Seattle, in 1984.

She is a Professor of physics at North Carolina State University, Raleigh. After a year-long appointment as a NATO Postdoctoral Fellow at the University d'Aix-Marseille II, France, she joined the Physics Department faculty at Northeastern University. She moved to North Carolina State University in 1998. Her research interests include solid-film growth processes and topologies at submicrometer length scales, surface processes in MEMS devices, nanotribology (the study of friction, wear, and lubrication at nanometer length and time scales), and liquid-film wetting phenomena. She is the director of the AFOSR-supported Extreme Friction MURI program and a co-PI of the DARPA-funded Center for RF MEMS Reliability.

Michael T. Dugger received the Ph.D. degree in materials science and engineering from Northwestern University, Chicago, IL, in 1990.

He is currently a Distinguished Member of the Technical Staff at Sandia National Laboratories, Albuquerque, NM, where he conducts a wide range of fundamental to applied research in tribology. Research topics include friction and wear in microelectromechanical systems, vapor phase lubrication, friction and wear in hard coatings, aging and performance of solid lubricants, particle generation due to wear, and the relationship between the mechanical and electrical behaviors of electrical contacts.